Magnetic properties of bulk Fe-doped indium oxide

2007 J. Phys.: Condens. Matter 19 236224

(http://iopscience.iop.org/0953-8984/19/23/236224)

IOP PUBLISHING JOURNAL OF PHYSICS: CONDENSED MATTER

J. Phys.: Condens. Matter **19** (2007) 236224 (9pp) doi:10.1088/0953-8984/19/23/236224

Magnetic properties of bulk Fe-doped indium oxide

David Bérardan[1] **and Emmanuel Guilmeau**

CRISMAT Laboratory, UMR 6508 CNRS-ENSICAEN, 6 Boulevard du Maréchal Juin, 14050 CAEN Cedex, France

E-mail: david.berardan@ensicaen.fr and emmanuel.guilmeau@ensicaen.fr

Received 14 March 2007, in final form 25 April 2007
Published 16 May 2007
Online at stacks.iop.org/JPhysCM/19/236224

Abstract

This paper presents the influence of the iron fraction and of the sintering atmosphere on the magnetic properties of bulk iron-doped indium oxide $In_{2-x}Fe_xO_3$. The formation of a solid solution between β-Fe_2O_3 and In_2O_3 up to $x \sim 0.3$ under argon atmosphere and $x \sim 0.55$ under air has been evidenced. All single-phase samples are paramagnetic, with dominant antiferromagnetic interactions and a paramagnetic effective moment originating from Fe^{3+} ions. For the higher x values, a cluster glass or superparamagnetic behaviour can be closely linked to the presence of Fe_2O_3 or Fe_3O_4 inclusions. No trace of ferromagnetism has been detected, even with samples prepared under argon.

1. Introduction

Since the theoretical prediction by Dietl *et al* [1] that ferromagnetism could be obtained above room temperature in manganese-doped semiconductors, intense research has been devoted to the study of diluted magnetic semiconductors (DMSs) due to their potential spintronics applications [2]. Many candidates have been discovered that could fulfil the requirements of high Curie temperature and independently controllable carrier density and magnetic doping. Several of them belong to the transparent conducting oxide (TCO) family, such as transition metal doped ZnO [3], TiO_2 [4], SnO_2 [5] and In_2O_3. For the development of a transparent conductive ferromagnetic material, In_2O_3 is one of the most promising candidates as host material as it is a widely industrially used TCO. Indeed, In_2O_3 is a wide band gap semiconductor (3.5–4.3 eV) [6] with a cubic bixbyite crystal structure [7]. Its electrical conductivity can be easily tuned by introducing oxygen vacancies and/or Sn doping.

In recent years, many authors have reported that room-temperature ferromagnetism can be achieved in transition metal doped indium oxide or indium tin oxide, the transition metals including Cr [8, 9], Mn [10], Fe [11, 12], Co [13] and Ni [14]. However, the magnetic properties strongly depend on the substrate nature and/or the synthesis process, and it seems that the ferromagnetism is somehow linked to oxygen vacancies (see for example [12]) in the

[1] Author to whom any correspondence should be addressed.

same manner as it has been shown in Ni-doped SnO_2 [15]. Nevertheless, the origin of the ferromagnetism in these materials and the physics underlying it remain controversial. The proposed origins include notably isolated clusters with charge transfer superexchange [16], mobile-electron-mediated coupling [17] or nanoscale ferromagnetic clusters [12]. Moreover, despite the dramatic influence of the synthesis conditions on the magnetic properties, most of these reports deal with thin films or nanocrystalline samples, and very few studies have been devoted to bulk materials, which could be less sensitive to the synthesis process. The magnetic properties of iron-doped indium oxide $In_{2-x}Fe_xO_3$ have been explored previously by several groups, who observed ferromagnetism in thin films annealed under argon [13] or with Cu co-doping [11], or a spin-glass behaviour in bulk samples prepared via a precipitation route and annealed under oxygen [18]. Therefore, we decided to investigate the magnetic properties of this system, and to study the influence of the iron fraction and the sintering atmosphere on the magnetic properties of bulk samples.

2. Experiments

All samples, belonging to the $In_{2-x}Fe_xO_3$ series, were prepared using a standard solid reaction route. Starting powders, In_2O_3 (Neyco, 99.99%) and Fe_2O_3 (Rectapur, 99%), were weighed in stoichiometric amounts and ground together by ball milling using agate balls and vial. The resulting powders were pressed uniaxially under 300 MPa, using polyvinyl alcohol binder to form parallelepipedic samples. Then they were sintered at 1350 °C for 24 h under air or argon atmosphere on platinum foils to avoid any contamination from the alumina crucible.

X-ray powder diffraction (XRD) was employed for structural characterization using a Philips X'Pert Pro diffractometer with Cu Kα radiation in a 2θ range 10°–90°. The XRD patterns were analysed using the Rietveld method with the help of the FullProf software [19].

The scanning electron microscopy (SEM) observations were made using an FEG Zeiss Supra 55 microscope. The cationic compositions were determined by wavelength dispersive spectroscopy (WDS) analysis (EDAX) using InAs (In Kα) and Fe (Fe_L) standards.

Thermal variations of the magnetic susceptibility ($\chi(T)$) and magnetization versus field curves ($M(H)$) were measured using a Quantum Design MPMS SQUID magnetometer between 2 and 300 K.

3. Results and discussion

The synthesis process presented above leads to well-crystallized samples, most of them being single phase, as exemplified in figure 1. This figure shows the Rietveld refinement of the x-ray diffraction pattern for a sample with the nominal composition $In_{1.7}Fe_{0.3}O_3$ sintered under air. All peaks can be indexed in the bixbyite structure type (space group $Ia3$, No. 206) and no trace of secondary phases can be detected within the estimated XRD detection limit. As summarized in table 1, the lattice parameter decreases with increasing iron fraction, which is consistent with the smaller ionic radius of Fe^{3+} as compared to In^{3+} [20]. The inset of figure 1 shows the evolution of the lattice parameter with the nominal iron fraction in $In_{2-x}Fe_xO_3$, for samples sintered under air or argon. The solid line represents Vegard's law between $a = 10.117$ Å for In_2O_3 [7] and $a = 9.393$ Å for β-Fe_2O_3 [21]. This Vegard's law is well followed until $x = 0.3$ for samples sintered under argon and $x = 0.5$ for samples sintered under air. From this picture, it seems that the solubility limit for Fe^{3+} in In_2O_3 depends on the sintering atmosphere, with a solubility limit as high as 27% for samples sintered under air. The same solubility limit has been reported previously by Ben-Dor *et al* [21]. As Fe^{2+} does not substitute for In^{3+} in In_2O_3 in

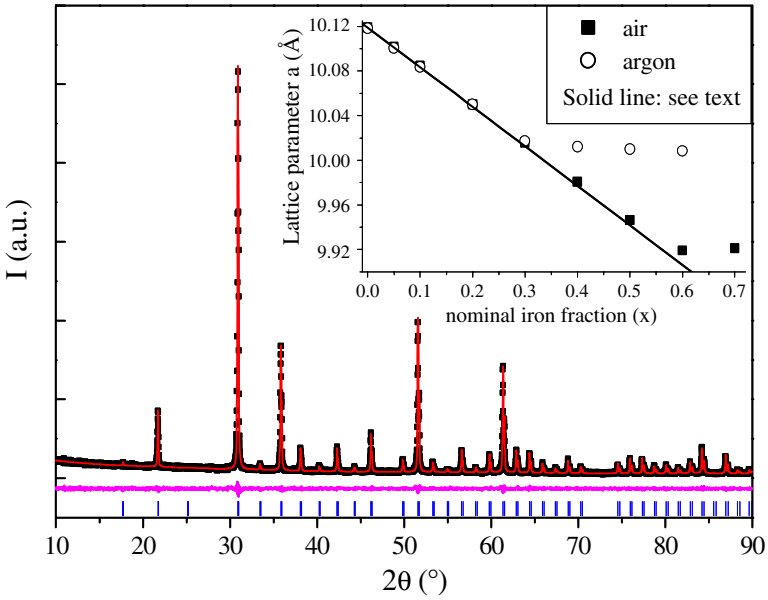

Figure 1. Rietveld refinement of the x-ray diffraction pattern for a sample ($x = 0.3$) sintered under air. Inset: lattice parameter versus nominal iron fraction in the series $In_{2-x}Fe_xO_3$ (open symbols: samples sintered under argon, filled symbols: samples sintered under air). The solid line represents Vegard's law between In_2O_3 [7] and β-Fe_2O_3 [21].

(This figure is in colour only in the electronic version)

Table 1. Nominal compositions, measured compositions (WDS), lattice parameter, effective magnetic moment (μ_{eff}) and paramagnetic temperature (θ_P) for the samples sintered under air. The oxygen content has been arbitrarily fixed as $(InFe)_2O_3$.

Nominal composition	WDS composition	Lattice parameter (Å)	Effective paramagnetic moment (μ_B)	Paramagnetic temperature (K)
In_2O_3		10.1188	Diamagnetic	Diamagnetic
$In_{1.95}Fe_{0.05}O_3$	$In_{1.952}Fe_{0.048}O_3$	10.1015	1.2	−3
$In_{1.9}Fe_{0.1}O_3$	$In_{1.904}Fe_{0.096}O_3$	10.0846	1.9	−59
$In_{1.8}Fe_{0.2}O_3$	$In_{1.81}Fe_{0.19}O_3$	10.0498	2.4	−67
$In_{1.7}Fe_{0.3}O_3$	$In_{1.71}Fe_{0.29}O_3$	10.0155	2.9	−118
$In_{1.6}Fe_{0.4}O_3$	$In_{1.61}Fe_{0.39}O_3$	9.9807	3.3	−148
$In_{1.5}Fe_{0.5}O_3$	$In_{1.51}Fe_{0.49}O_3$	9.9462	3.7	−176
$In_{1.4}Fe_{0.6}O_3$	$In_{1.51}Fe_{0.49}O_3$ + Fe_xO_y	9.9209	Cluster glass or superparamagnetic	Cluster glass or superparamagnetic

significant amounts (we tried to perform In^{3+} substitution by Fe^{2+} using FeO as starting powder without success), the solubility difference upon sintering atmosphere probably originates from a partial reduction of Fe_2O_3 starting powder under argon atmosphere.

Above this solubility limit, secondary phases can be detected in the x-ray diffraction patterns. Figure 2 shows a magnified view of the XRD patterns in the series $In_{2-x}Fe_xO_3$ with x increasing from 0.05 to 0.6 from bottom to top (left: samples sintered under air, right: samples sintered under argon). The sample with the nominal composition $In_{0.4}Fe_{0.6}O_3$ sintered under air unambiguously contains a small amount of Fe_2O_3 hematite (peak indicated by a square symbol

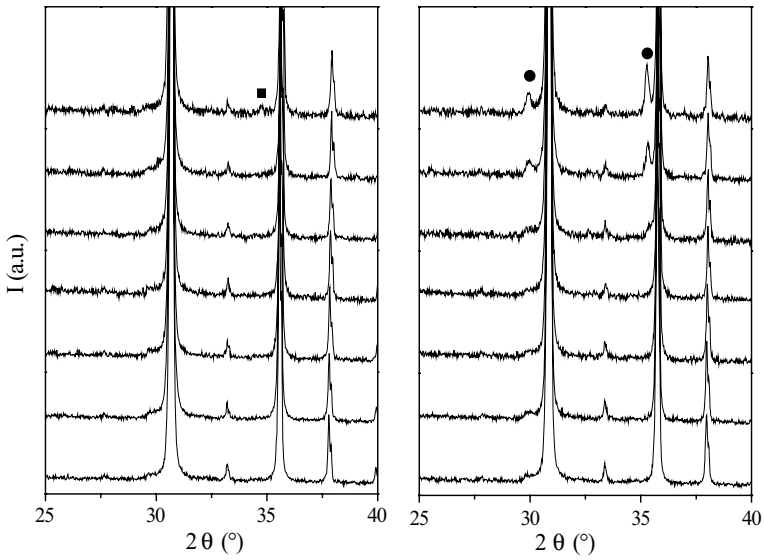

Figure 2. Magnified views of x-ray diffraction patterns for samples with different x (from bottom to top: $x = 0.05, 0.1, 0.2, 0.3, 0.4, 0.5, 0.6$). Left: samples sintered under air, right: samples sintered under argon. The square symbol corresponds to a Fe_2O_3 hematite Bragg reflection, and the circle symbols correspond to Fe_3O_4 magnetite Bragg reflections.

on the XRD pattern), whereas all samples with $x > 0.3$ sintered under argon contains a small amount of Fe_3O_4 magnetite (peaks indicated by a circle symbol on the XRD patterns). As both hematite and magnetite are magnetic materials, we will see that small residual amounts in the samples dramatically influence their magnetic properties.

This result was confirmed by SEM observations since the presence of iron oxide secondary phases was clearly identified (figure 3). Bellow the solubility limit determined by XRD, no secondary phases can be seen in the pictures, whereas above this limit the samples unambiguously contain secondary phases, identified as iron oxide by WDS analysis. Moreover, the WDS analysis performed on all samples showed that, bellow the solubility limit, the grain compositions are very close to the nominal ones (see table 1), which confirms that Fe^{3+} does substitute In^{3+} in In_2O_3.

To check that no contamination by magnetic impurities occurred during the synthesis process, the magnetic behaviour of undoped In_2O_3 was recorded. Both samples, sintered under air or argon, are diamagnetic, as expected for bulk indium oxide (not shown). For iron-doped samples, two distinct behaviours can be observed. First, all the samples below the solubility limit are paramagnetic, whatever the sintering atmosphere. Although the argon sintering induces oxygen vacancies [22], it does not lead to ferromagnetism. Figure 4 shows a typical example of the magnetic behaviour observed in these compounds, with $x = 0.2$. The inverse magnetic susceptibility $(1/\chi)$ increases linearly with temperature above $\sim$100 K, the field-cooled and zero-field-cooled curves are identical, and the paramagnetic behaviour can be easily described using a classical Curie–Weiss law. Moreover, the curve does not display any characteristic feature of a transition to a magnetic order. The inset shows a magnetization versus field curve, which is linear too. This behaviour is very different from the results reported by Hong *et al* [13] and Kohiki *et al* [18], as will be discussed later.

In figure 5 are displayed the temperature dependences of the zero-field-cooled susceptibility χ_{ZFC} and field-cooled susceptibility χ_{FC} for a sample exceeding the solubility

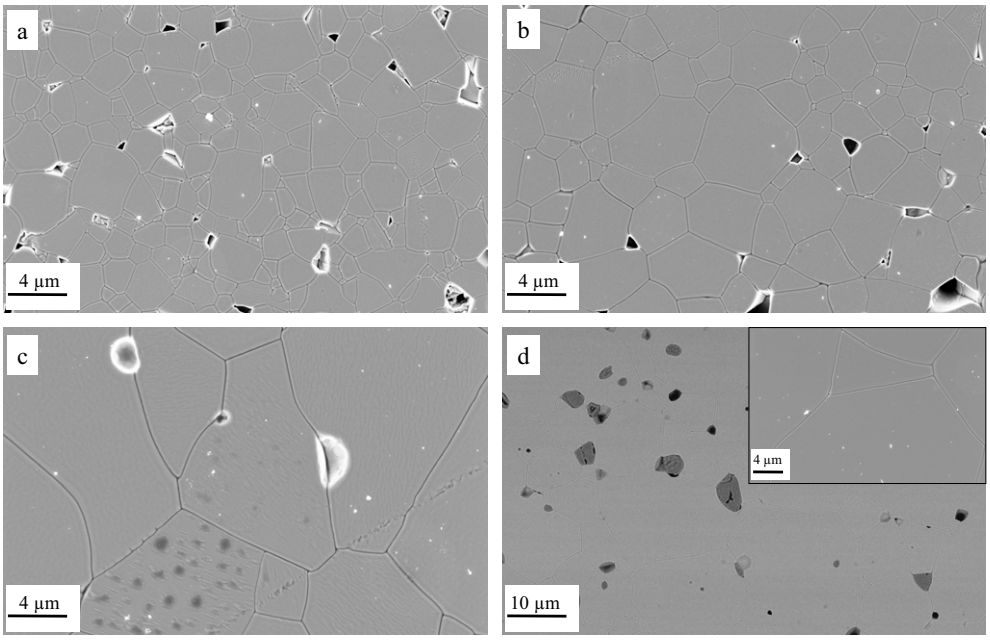

Figure 3. SEM images of samples with different x (a: $x = 0.05$, b: $x = 0.2$, c: $x = 0.4$, d: $x = 0.6$). Dark areas on image (d) correspond to iron oxide inclusions. Inset in image (d) corresponds to the same magnification as images (a), (b) and (c).

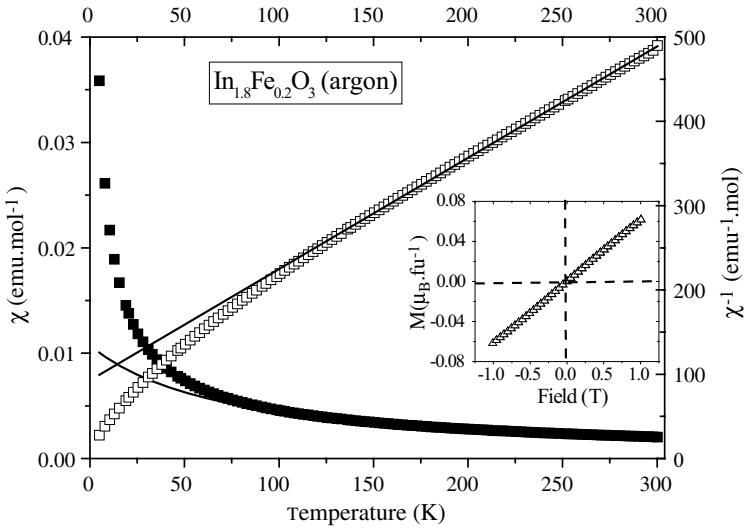

Figure 4. Magnetization versus temperature ($H = 100$ Oe) for a sample with the nominal composition $In_{1.8}Fe_{0.2}O_3$ sintered under argon atmosphere. The solid lines are fitted assuming a Curie–Weiss law. Inset: magnetization versus field at 5 K.

limit. χ_{FC} increases linearly with decreasing temperature from room temperature to ~100 K, whereas χ_{ZFC} deviates from χ_{FC} with decreasing temperature. It is noteworthy that χ_{ZFC} already deviates from χ_{FC} around room temperature. The inset of figure 5 shows the magnetization

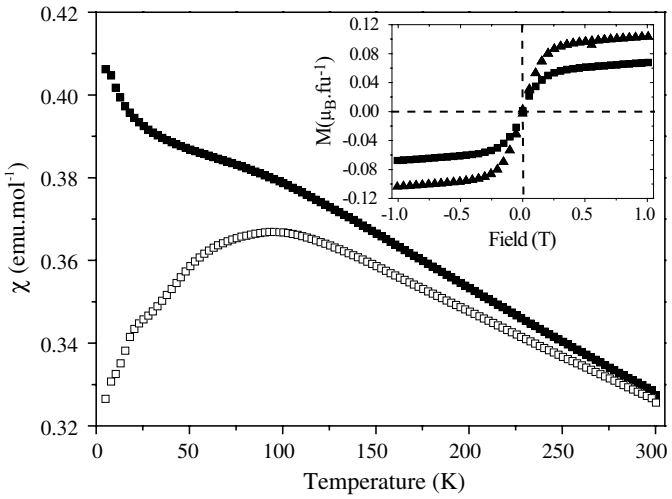

Figure 5. Magnetization versus temperature at 100 Oe for a sample with nominal composition $In_{1.4}Fe_{0.6}O_3$ sintered under air (filled symbols: χ_{FC}, open symbols: χ_{ZFC}). Inset: magnetization versus field curves for two samples with the same final composition but different Fe_2O_3 fractions.

versus field curve recorded at 5 K for the same sample (square symbols) and for another sample with same final composition but slightly higher Fe_2O_3 fraction as deduced from XRD refinement and SEM observations (triangle symbols). It has unambiguously a sigmoid shape, but no hysteresis or spontaneous magnetization can be seen, which evidences the absence of long-range magnetic ordering. It is noteworthy that the observed values for the saturation moment can be reasonably explained assuming the presence of a few per cent of Fe_2O_3, which is consistent with the XRD patterns. Moreover, a slightly higher Fe_2O_3 content for a similar $In_{2-x}Fe_xO_3$ composition corresponds to a slightly higher saturation moment. We thus believe that this behaviour is extrinsic and directly linked to the presence of Fe_2O_3 (under air) or Fe_3O_4 (under argon) inclusions randomly dispersed in the matrix, that induce a cluster glass or superparamagnetic behaviour [23].

Figure 6 shows the effect of the iron fraction on the paramagnetic temperature θ_p and on the effective paramagnetic moment μ_{eff} obtained from the Curie–Weiss law. All parameters are summarized in table 1. Once again, no difference can be detected between samples sintered under argon and air despite the oxygen vacancies induced by argon sintering. θ_p is negative and linearly decreases with increasing iron fraction, denoting dominant antiferromagnetic interactions. This behaviour is consistent with the results reported by Kohiki *et al* [18], who showed that the spin density of states (DOS) of Fe^{3+} ions located in 8b and 24d sites in $In_{2-x}Fe_xO_3$ are asymmetric and that the superexchange interaction between Fe^{3+} ions leads to antiferromagnetic behaviour. Moreover, it has been reported that β-Fe_2O_3 is antiferromagnetic with Néel temperature $T_N = 119$ K [24]. The dilution of β-Fe_2O_3 in In_2O_3 to form the solid solution $In_{2-x}Fe_xO_3$ lowers the antiferromagnetic coupling between Fe^{3+} atoms, and the compounds remain in a paramagnetic state. This coupling increases as the Fe^{3+} concentration increases and as the Fe^{3+} ions become closer to one another, which leads to the increase of the absolute value of θ_p. The paramagnetic effective moment increases with increasing iron fraction x, following the relation

$$\mu_{eff}^2 = xA^2,$$

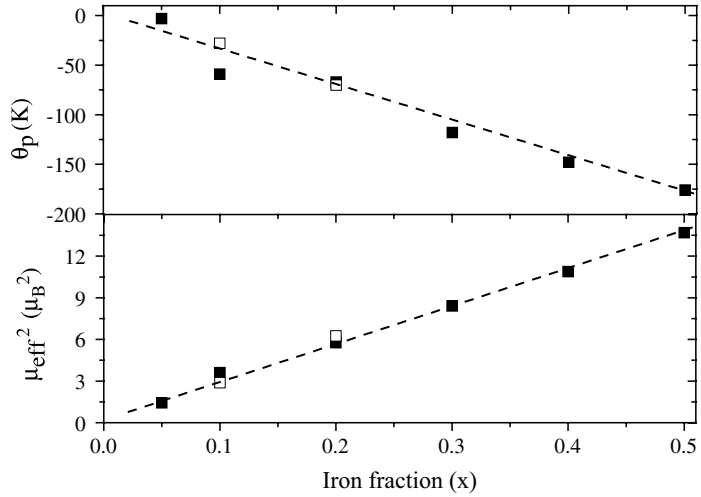

Figure 6. Top: evolution of the paramagnetic temperature θ_p with the iron fraction in the series $In_{2-x}Fe_xO_3$ sintered under air (filled symbols) or argon (open symbols). Bottom: evolution of the square of effective paramagnetic moment with the iron fraction. Dashed lines are linear fits.

with $A = 5.2\mu_B$ obtained from a linear fit of the data. This value is reasonably consistent with a paramagnetic behaviour only originating from Fe^{3+} atoms weakly interacting.

From our results, we can conclude that bulk iron-doped indium oxide is paramagnetic, even with argon sintering. The cluster glass or superparamagnetic behaviour observed for high iron concentrations clearly originates from the presence of randomly dispersed ferromagnetic inclusions of Fe_2O_3 or Fe_3O_4. These results strongly disagree with those reported by Kohiki *et al* [18] and Hong *et al* [13]. The first group reported a cluster glass behaviour with $T_F \sim 280$ K in $In_{1.85}Fe_{0.15}O_3$ prepared by a coprecipitation route as well as a cusp in $\chi(T)$ curves at 30 K attributed to superexchange interactions between Fe^{3+} atoms. However, they reported for their sample a lattice parameter ($a = 10.088$ Å) that does not correspond to the nominal composition, but rather to $In_{1.92}Fe_{0.08}O_3$. We strongly believe that the magnetic properties observed in their sample are extrinsic and originate from the presence of randomly dispersed unreacted nanocrystalline Fe_2O_3. Hong *et al*, however, reported room-temperature ferromagnetism in transition metal (TM) doped In_2O_3 thin films with TM = V, Cr, Fe, Co, Ni. As their magnetic force microscopy (MFM) measurements ruled out the possibility that the ferromagnetism could originate from clusters in their samples, it is most probably intrinsic. As our samples are unambiguously paramagnetic, the question of the origin of the magnetic behaviour of TM-doped In_2O_3 remains open. The best way to test the intrinsic nature of ferromagnetism in DMSs is usually to check the presence of an anomalous Hall effect (AHE); see for example [17]. Indeed, magnetic contributions to the Hall effect originate from the matrix and not from dispersed inclusions. However, it has been shown recently that the AHE and nanosized cluster driven superparamagnetism can coexist in Co-doped TiO_2 films [25]. Moreover, Sundaresan *et al* [26] and Hong *et al* [27] reported recently the occurrence of ferromagnetism in undoped nanoparticles or thin-film oxides that were otherwise nonmagnetic. Even more surprising, the second group reported a degradation of magnetic ordering in In_2O_3 thin films with Mn or Cu doping [28]. Thus, it seems that, in indium oxide thin films or nanocrystalline samples prepared under special conditions, ferromagnetism does not originate from the dopant but from an intrinsic behaviour of the matrix, which could be the equivalent

for d^{10} elements of the so-called d^0 ferromagnetism [29]. As oxygen vacancies seem to be a key feature for such unexpected ferromagnetism to occur [15], the discrepancy between the magnetic properties of bulk samples on the one hand and of nanocrystalline samples or thin films on the other hand may originate from a different surface/volume ratio. This different surface/volume ratio certainly leads to different oxygen diffusion through the samples inducing different oxygen vacancies concentrations, which directly influences the electronic band structure. Thus, it would be of great interest to carefully study the effect of oxygen stoichiometry and grain size or dimensionality of doped and undoped indium oxide samples on their magnetic properties. New investigations are under way which focus on this topic.

4. Conclusions

We have shown that bulk iron-doped indium oxide samples belonging to the series $In_{2-x}Fe_xO_3$ are paramagnetic, even when sintered under argon. The dominant interactions are antiferromagnetic and the paramagnetic effective moment only originates from Fe^{3+} ions. A cluster glass or superparamagnetic behaviour for high iron fractions has been linked to the presence of randomly dispersed Fe_2O_3 or Fe_3O_4 inclusions. We strongly believe that the discrepancy between these results and those reporting ferromagnetism in thin films or nanocrystalline samples is closely linked to different surface/volume ratios and therefore to different oxygen vacancy concentrations. The ferromagnetism observed in low-dimensionality samples probably originates from intrinsic properties of the host In_2O_3 matrix rather than from the dopant. Further work is currently under way to investigate the effect of grain size on the magnetic properties.

Acknowledgments

We acknowledge Dr S Hebert for fruitful discussions. EG gratefully acknowledges the French Ministère de la Recherche et de la Technologie and the Délégation Régionale à la Recherche et à la Technologie—région Basse Normandie—for financial support.

References

[1] Dietl T, Ohno H, Matsukura F, Cibert J and Ferrand D 2000 *Science* **287** 1019
[2] Wolf S A, Awschalom D D, Buhrman R A, Daughton J M, von Molnár S, Roukes M L, Chtchelkanova A Y and Treger D M 2001 *Science* **294** 1488
[3] Venkatesan M, Fitzgerald C B, Lunney J G and Coey J M D 2004 *Phys. Rev. Lett.* **93** 177206
[4] Matsumoto Y, Murakami M, Shono T, Hasegawa T, Fukumura T, Kawasaki M, Ahmet P, Chikyow T, Koshihara S and Koinuma H 2001 *Science* **291** 854
[5] Ogale S B *et al* 2003 *Phys. Rev. Lett.* **91** 077205
[6] Weiher R L and Ley R P 1966 *J. Appl. Phys.* **37** 299
[7] Marezio M 1966 *Acta Crystallogr.* **20** 723
[8] Philip J, Punnoose A, Kim B I, Reddy K M, Layne S, Holmes J O, Satpati B, Leclair P R, Santos T S and Moodera J S 2006 *Nat. Mater.* **5** 298
[9] Kim H S, Ji S H, Kim H, Hong S K, Kim D, Ihm Y E and Choo W K 2006 *Solid State Commun.* **137** 41
[10] Philip J, Theodoropoulou N, Berera G, Moodera J S and Satpati B 2004 *Appl. Phys. Lett.* **85** 777
[11] He J, Xu S, Yoo Y K, Xue Q, Lee H C, Cheng S, Xiang X D, Dionne G F and Takeuchi I 2005 *Appl. Phys. Lett.* **86** 052503
[12] Ohno T, Kawahara T, Tanaka H, Kawai T, Oku M, Okada K and Kohiki S 2006 *Japan. J. Appl. Phys.* **45** L957
[13] Hong N H, Sakai J, Huong N T, Ruyter A and Brizé V 2006 *J. Phys.: Condens. Matter* **18** 6897
[14] Peleckis G, Wang X and Dou S X 2006 *Appl. Phys. Lett.* **89** 022501
[15] Hong N H, Sakai J, Huong N T, Poirot N and Ruyter A 2005 *Phys. Rev.* B **72** 045336

[16] Yoo Y K *et al* 2005 *Appl. Phys. Lett.* **86** 042506
[17] Yu Z G, He J, Xu S, Xue Q, van't Erve O M J, Jonker B T, Marcus M A, Yoo Y K, Cheng S and Xiang X D 2006 *Phys. Rev.* B **74** 165321
[18] Kohiki S *et al* 2006 *Thin Solid Films* **505** 122
[19] Rodriguez-Carjaval J 1993 *Physica* B **192** 55
[20] Shannon R D 1976 *Acta Crystallogr.* A **32** 751
[21] Ben-Dor L, Fischbein E, Felner I and Kalman Z 1977 *J. Electrochem. Soc.* **124** 451
[22] De Wit J H W 1975 *J. Solid State Chem.* **13** 192
[23] Mydosh J A 1993 *Spin Glasses: An Experimental Introduction* (London: Taylor and Francis)
[24] Ikeda Y, Takano M and Bando Y 1986 *Bull. Inst. Chem. Res., Kyoto Univ.* **64** 249
[25] Shinde S R, Ogale S B, Higgins J S, Zheng H, Millis A J, Kulkarni V N, Ramesh R, Greene R L and Venkatesan T 2004 *Phys. Rev. Lett.* **92** 166601
[26] Sundaresan A, Bhargavi B, Rangarajan N, Siddesh U and Rao C N R 2006 *Phys. Rev.* B **74** 161306
[27] Hong N H, Sakai J, Poirot N and Brizé N 2006 *Phys. Rev.* B **73** 132404
[28] Brizé V, Sakai J and Hong N H 2007 *Physica* B **392** 379
[29] Venkatesan M, Fitzgerald C B and Coey J M D 2004 *Nature* **430** 630